Journal of Physics D: Applied Physics

LETTER

Resistance change of stretchable composites based on inkjet-printed silver nanowires

IOP Publishing
Letters
Journal of Physics D: Applied Physics
J. Phys. D: Appl. Phys. **53** (2020) 05LT02 (6pp)
https://doi.org/10.1088/1361-6463/ab524d

Letter

Resistance change of stretchable composites based on inkjet-printed silver nanowires

Xiaowen Xu[1], Guanghui Han[1,2], Haoran Yu[2], Xiao Jin[2], Junliang Yang[1], Jian Lin[2] and Changqi Ma[2]

[1] Hunan Key Laboratory for Super-Microstructure and Ultrafast Process, School of Physics and Electronics, Central South University, Changsha 410083, People's Republic of China
[2] Printable Electronics Research Centre, Suzhou Institute of Nano-Tech and Nano-Bionics, Chinese Academy of Sciences, No. 398 Ruoshui Road, SEID, Suzhou Industrial Park, Suzhou, Jiangsu Province, 215123, People's Republic of China

E-mail: junliang.yang@csu.edu.cn and jlin2010@sinano.ac.cn

Received 25 July 2019, revised 14 October 2019
Accepted for publication 29 October 2019
Published 25 November 2019

Abstract

The fluctuation of the stretched resistance of composites based on inkjet-printed silver nanowires (AgNW) and polydimethylsiloxane (PDMS) is controlled by different ratios of a curing agent in PDMS, with an optimized normalized resistance change as low as 4.67% in a 50% tensile testing cycle. The results confirm that the properties of PDMS including the Young's modulus and creep deformation play key roles in controlling the resistance changes of stretched AgNW–PDMS composites based on inkjet-printed AgNW, which opens up applications of inkjet-printable elastic AgNW conductors in stretchable electronics.

Keywords: silver nanowire–elastomer composite, stretchable, inkjet printed, resistance change, Young's modulus

(Some figures may appear in colour only in the online journal)

1. Introduction

To overcome the mismatch between biology and traditional rigid electronics, there has been a growing interest in soft and elastic electronic systems [1] such as electronic skin and wearable electronics [2–4]. As a result, stretchable conductors with a controlled resistance change are necessary for fabricating the integrated circuit interconnects or sensors in electronic skin or wearable electronics. Considering the typical stretchability of human skin is no more than 30% [5, 6] as well as the non-stretchable areas in hybrid electronics [7], the conductive lines and interconnectors of a wearable circuit should have a strain range of about 50%. To yield stretchability, some stiff thin conductive films were reported to be buckled by obtaining wavy structures by pre-stretching [8], or formed serpentine [9], helical [10], and spiral [11] strategic structures through cutting techniques such as origami [12] and kirigami [13]. New materials or composites based on liquid metals [14], carbon materials [15], and silver materials [16] also have been reported as stretchable conductors.

Composites based on conductive networks of one-dimensional (1D) materials, including carbon nanotubes [17] and silver nanowires (AgNW) [18], have inherent advantages in integrating with elastomers [19] to produce stretchable conductive materials [20] due to a much lower volume ratio in the composite. A typical example is the composite reported in [21] with spontaneous buckling after stretching–releasing cycles that are due to the irreversible sliding of the AgNW embedded just below the surface of polydimethylsiloxane (PDMS).

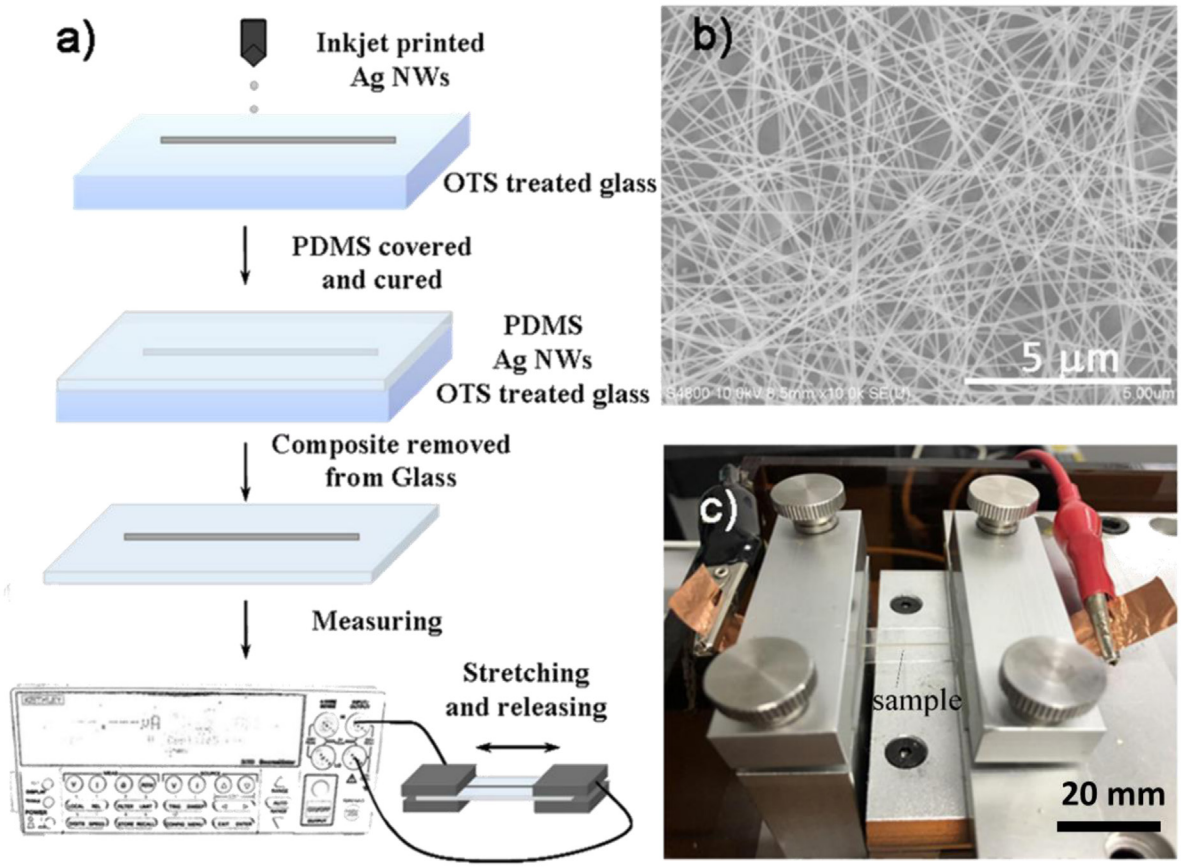

Figure 1. Schematic diagram of the AgNW–PDMS composites' fabrication and measurement (a), as well as an SEM image of the printed AgNW (b) and the connection method of the resistance measurement (c).

A AgNW conductive network, which has a better conductivity than carbon nanotubes, can be deposited by non-patterned methods such as a slot die [22], spraying [23], a Mayer rod [24] or off-center spin-coating [25], as well as patterned methods including oxygen plasma treatment via a shadow mask [26], capillary force lithography [27], laser cutting [28], water-bath pulling [29], screen printing [30] and gravure printed AgNW [31]. Thanks to the advantages of digital control and a non-contact mode, nozzle-based printing methods including inkjet [32, 33], electrohydrodynamic jet [34, 35], 3D [36] and aerosol jet [37] printing can be the most versatile printing methods for the fabrication of soft and elastic electronics. It should be possible to inkjet print AgNW–PDMS composites for electronics applications because both AgNW [38] and PDMS [39] can be printed. However, there has been not yet been a report focused on the stretchable conductive properties of elastic composites based on inkjet-printed 1D materials such as AgNW. In this work, the resistance change of AgNW–PDMS composites based on inkjet-printed AgNW is studied using PDMS with different properties.

2. Methods

A AgNW suspension in ethanol was purchased from Gu's Materials, with a diameter of about 55–80 nm, and length of 20–40 μm. The suspension was then diluted to 1 mg ml^{-1} with ethanol, and inkjet-printed by a MicroFab Jetlab II inkjet printer with a 50 μm diameter printhead on octadecyltrichlorosilane (OTS) pre-treated glass substrates. The OTS self-assembled monolayer on the glass was used to form finer and more uniform printed AgNW lines, as well as the facilitated separation of the cured PDMS film. The printed AgNW lines (about 0.5–0.6 μm thick, measured by VEECO, DEKTAK 150) were dried on a hotplate at 120 °C for 5 min. Then, the PDMS precursor mixture with a cross-linker (Dow Corning Sylgard 184, with the weight ratio of the base to the cross-linker changed from 5:1 to 20:1) was poured on the printed AgNW. To give a sufficient contact with the printed AgNW, the PDMS precursor was kept for 1 h without any movement or heating. After a curing process of 60 °C for 3 h, the samples (about 0.6 mm thick) were removed from glass for tensile testing. The Young's modulus was measured

Table 1. The average resistance values (Ω) of samples.

PDMS ratio	5:1	10:1	15:1	20:1
AgNW before pouring PDMS	30.12	30.24	31.02	30.3
PDMS–AgNW removed from glass	51.88	111.4	339.76	462.06
Before 50% stretched PDMS–AgNW	63.73	118.5	349.0	679.91

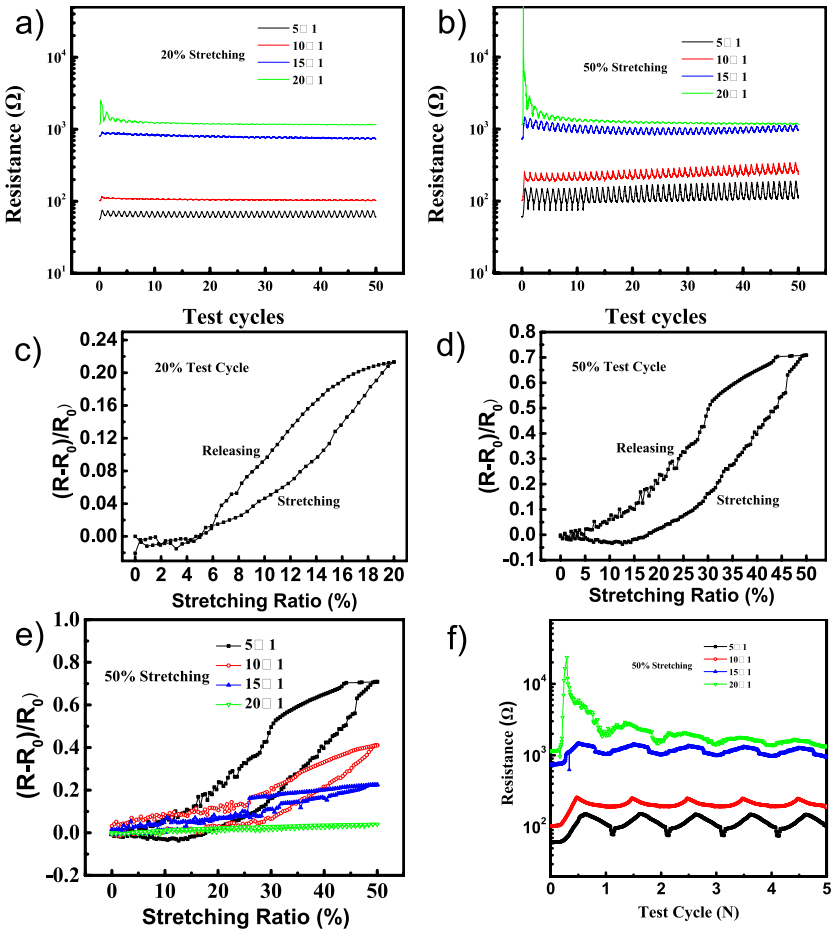

Figure 2. (a), (b) The resistances of samples during the test cycles with stretching ranges of 20% and 50% respectively. (c) The normalized change ratios of the sample with 5:1 PDMS during the test cycles with different stretching. (d) The R_{NC} curves of different samples during typical 50% stretching test cycles. (e) The resistance change of different samples during the first five test cycles with 50% stretching.

Table 2. The comparison of PDMS and R_{NC} at 50% stretching.

Composite	A	B	C	D
PDMS ratio	5:1	10:1	15:1	20:1
Young's modulus of PDMS (GPa)	1.289	0.487	0.258	0.135
Creep deformation	2%	1.8%	1.5%	1%
Typical R_{NC}	73.24%	41.75%	22.21%	4.67%

using a universal testing machine bought from Shanghai Hualong Test Instruments Corporation. The samples were stretched and released automatically at a speed of 20 mm min^{-1} by a self-made machine for 20% and 50% elongation in sequence. Meanwhile, the varied resistances during the stretching–releasing process (a test cycle) were measured and recorded in real-time during the measurements by a Keithley 2400 sourcemeter with a constant output voltage of 1 V. An atomic force microscope (AFM; Dimension Icon) and a scanning electron microscope (SEM; Hitachi S-4800) were used for the measurement observations. A schematic diagram of the AgNW–PDMS composites' fabrication and measurement, an SEM image of the printed AgNW, as well as the connection method of the resistance measurement, are shown in figure 1.

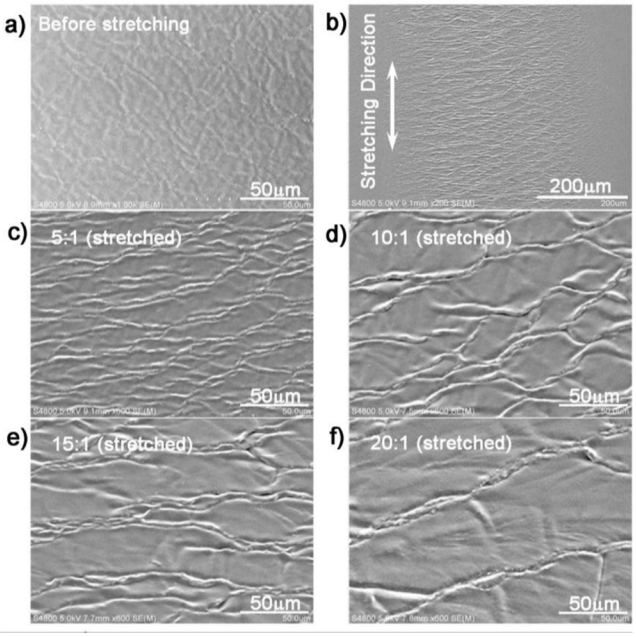

Figure 3. (a) SEM figure of the AgNW–PDMS surface without stretching. (b) The overview of wrinkles on the surface of printed AgNW–PDMS after 50% stretching. (c)– (f) SEM results of samples with different PDMS ratios after 50% stretched test cycles.

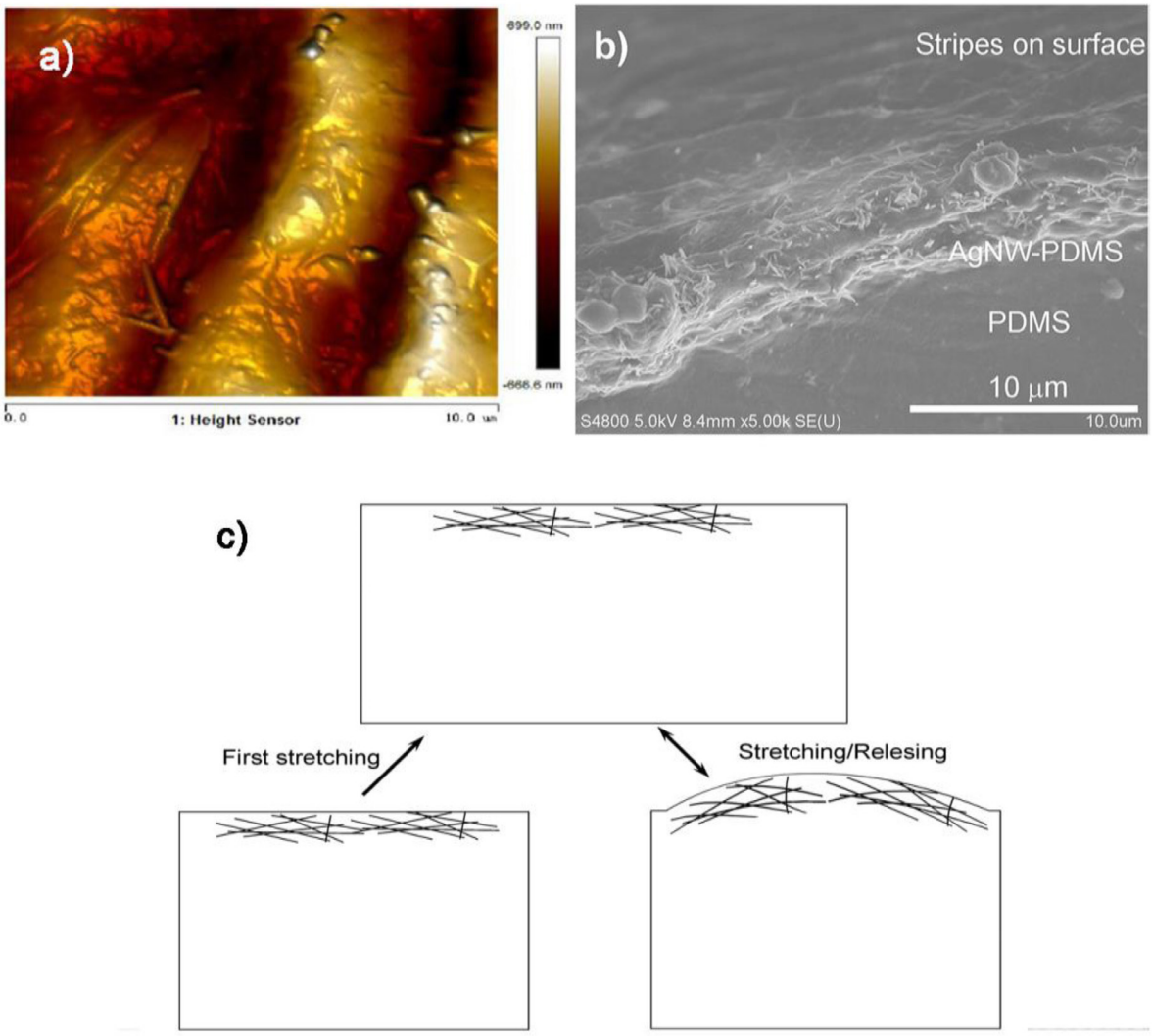

Figure 4. (a) The AFM image of the typical wrinkles on the sample surface. (b) The cross-sectional higher-magnification SEM figures with typical wrinkles on the AgNW–PDMS composite. (c) Schematic diagram of the stretching and releasing processes.

3. Results and discussion

Four kinds of AgNW–PDMS composites using PDMS mixing ratios of 5:1, 10:1, 15:1, and 20:1 were fabricated, called samples A, B, C, and D, respectively. To obtain details about the changes of AgNW–PDMS, a series of resistances had been measured in our experiment. Ten samples with the same fabrication methods (using different PDMS ratios of 5:1, 10:1, 15:1, and 20:1, respectively) were fabricated and measured, with the average resistance values shown in table 1. For example, the resistance of AgNW–PDMS removed from glass confirmed that AgNW–PDMS increased its resistance during the process of pouring PDMS, curing, and removing it from the glass. It can be found that the samples using 5:1 PDMS had the lowest resistance increase, while the AgNW with 20:1 PDMS had the highest increased values.

The resistances of composites were measured during 50 stretching and releasing test cycles with tensile ranges of 20% and 50%, with their typical overall views of resistances depicted in figures 2(a) and (b). The curves of resistance-testing cycles with a 20% stretching range are much smoother than for the 50% tensile test, demonstrating the larger resistance changes of the latter. On the other hand, as the ratio of the curing agent in PDMS decreased from 5:1 to 20:1, the resistance change ratio also showed a reducing trend with the decreasing content of the curing agent.

The normalized resistance change (R_{NC}, $(R - R_0)/R_0$) is used to calculate the resistance changes of composites, with the initial resistance value at the very start of the test cycle as R_0. Take sample A as an example, its R_{NC} is 22.69% during the 20% stretched cycle (left of figure 2(c)), and increases to about 73.24% when the measurement is in the tensile range of 50% (right of figure 2(c)). On the other hand, the typical R_{NC} curves of four different AgNW–PDMS composites measured during the 50% stretching test were analyzed in figure 2(d). It is obvious that there is a downward trend of R_{NC} from samples A to D. The typical R_{NC} values and Young's modulus of PDMS when at 50% stretched can also be found in table 2.

The resistances of four different AgNW–PDMS composites measured as a function of tensile strain during the first five testing cycles with 50% stretching are shown in figure 2(e). It can be found that the resistance changes in the first test cycle

are larger than others, which is similar to that reported in [21]. In other words, there are two kinds of conductivity variation, which can be distinguished as irreversible and reversible, in the first cycles. Most of the resistance changes belong to the latter in the next cycles. However, sample D has a very sharp resistance increase when it is 21%–29% strained, and the resistance drops irreversibly in about three testing cycles, which is obviously slower than in other samples.

The surface morphologies of AgNW–PDMS samples have also been explored. SEM figures show that the sample surface is quite smooth before being stretched (figure 3(a)). However, a series of wrinkles were found to occur perpendicular to the stretching direction of the composite (figure 3(b)). There are stripes with different densities on the AgNW–PDMS surface after the tensile test for the 50% elongation (figure 3(c)). The most wrinkles are on the surface of the composite using 5:1 PDMS, while the sample with the 20:1 PDMS ratio has the fewest wrinkles on its surface.

Due to the micron-scale thickness and opacity of printed AgNW, it is difficult for researchers to observe the movements of a whole AgNW network directly. However, the wrinkles' peak-to-valley height is found to be as large as 1.4 μm (figure 4(a)), and there is about 6% (v/v) unstretchable AgNW in the AgNW–PDMS composite layer (as shown in figure 4(b)). As a result, the PDMS in this composited layer, which is split into several parts, has obvious creep deformation during the stretching–releasing process. Therefore, the AgNW–PDMS composite layer which is one thousandth as thick as the adjacent pure PDMS layer has a much larger Young's modulus. Considering the inkjet-printed AgNW layer will be unavoidably heterogeneous in the density, there will be some points with a higher PDMS content in the composited layer, which is much more brittle than the PDMS layer. On the other hand, the wrinkles on the surface indicate creep deformation of the AgNW–PDMS thin composited layer. The components of the PDMS should play a key role in this kind of creep deformation. As a result, the sample using 5:1 PDMS, which has the highest creep deformation, has the most wrinkles after stretching.

Figure 4(c) shows the schematic diagram of the stretching and releasing processes. When the sample is stretched, the AgNW–PDMS thin layer was elongated. There are some micro-scale breaks in the AgNW network because of its brittleness. Considering the creep deformation of the AgNW–PDMS composited layer, most of these micro-scale breaks are irreversible. The composite using PDMS with a higher Young's modulus can protect the AgNW network during this process. This is why the sample with 5:1 PDMS has the smallest resistance changes in absolute value, and the composite using PDMS with a lower Young's modulus increased its resistance sharply. However, there are wrinkles on the AgNW–PDMS surface after the stretching–releasing cycle because of the creep deformation of a very thin composited layer. The AgNW network has very limited sliding or breakage during this process. Considering that the bonding between AgNW and PDMS may be inferior to the AgNW network under tensile strain, the PDMS ratio with a lower creep deformation can better protect the AgNW network from sliding or breakage. This is the reason why the sample using 20:1 PDMS has R_{NC} as low as 4.67% in a 50% tensile testing cycle.

4. Conclusion

PDMS composites based on inkjet-printed silver nanowires were fabricated for a stretchable conductive circuit. The results show that the properties of PDMS including its Young's modulus and creep deformation play key roles in controlling the resistance changes of stretched AgNW–PDMS. The sample using PDMS with a higher Young's modulus has a lower irreversible resistance change under the first stretching, while the composite using PDMS with a lower creep deformation has a smaller reversible R_{NC}. The stretchable composite based on inkjet-printed AgNW can reduce the R_{NC} to 4.67% in a 50% tensile testing cycle using PDMS with a ratio of 20:1. The results confirm that the properties of the elastomer play key roles in improving the conductivity of stretchable composites based on inkjet-printed AgNW, which opens up applications of inkjet-printable elastic AgNW conductors in functional devices.

Acknowledgments

This work was supported by the National Natural Foundation of China (Grant No. 21003153), and the Ministry of Science and Technology of China (Grant No. 2016YFA0200700).

ORCID iDs

Xiaowen Xu https://orcid.org/0000-0002-3169-5285
Junliang Yang https://orcid.org/0000-0002-5553-0186
Jian Lin https://orcid.org/0000-0002-3037-7023

References

[1] Rogers J A, Someya T and Huang Y G 2010 Materials and mechanics for stretchable electronics *Science* **327** 1603–7
[2] Liu Y, Pharr M and Salvatore G A 2017 Lab-on-skin: a review of flexible and stretchable electronics for wearable health monitoring *ACS Nano* **11** 9614–35
[3] Zamarayeva A M, Ostfeld A E, Wang M, Duey J K, Deckman I, Lechene B P, Davies G, Steingart D A and Arias A C 2017 Flexible and stretchable power sources for wearable electronics *Sci. Adv.* **3** e1602051
[4] Cheng Y, Wang R, Zhai H and Sun J 2017 Stretchable electronic skin based on silver nanowire composite fiber electrodes for sensing pressure, proximity, and multidirectional strain *Nanoscale* **9** 3834–42
[5] Arumugam V, Naresh M D and Sanjeevi R 1994 Effect of strain-rate on the fracture-behavior of skin *J. Biosci.* **19** 307–13
[6] Kim D H *et al* 2011 Epidermal electronics *Science* **333** 838–43
[7] Lee Y *et al* 2018 Wireless, intraoral hybrid electronics for real-time quantification of sodium intake toward hypertension management *Proc. Natl Acad. Sci. USA* **115** 5377–82
[8] Jones J, Lacour S P, Wagner S and Suo Z G 2004 Stretchable wavy metal interconnects *J. Vac. Sci. Technol.* A **22** 1723–5

[9] Pan T S, Pharr M, Ma Y J, Ning R, Yan Z, Xu R X, Feng X, Huang Y G and Rogers J A 2017 Experimental and theoretical studies of serpentine interconnects on ultrathin elastomers for stretchable electronics *Adv. Funct. Mater.* **27** 1702589
[10] Won Y, Kim A, Yang W, Jeong S and Moon J 2014 A highly stretchable, helical copper nanowire conductor exhibiting a stretchability of 700% *NPG Asia Mater.* **6** e132
[11] Wu X D, Han Y Y, Zhang X X and Lu C H 2017 Spirally structured conductive composites for highly stretchable, robust conductors and sensors *ACS Appl. Mater. Interfaces* **9** 23007–16
[12] Kim M, Park J, Ji S, Shin S H, Kim S Y, Kim Y C, Kim J Y and Park J U 2016 Fully-integrated, bezel-less transistor arrays using reversibly foldable interconnects and stretchable origami substrates *Nanoscale* **8** 9504–10
[13] Shyu T C, Damasceno P F, Dodd P M, Lamoureux A, Xu L Z, Shlian M, Shtein M, Glotzer S C and Kotov N A 2015 A kirigami approach to engineering elasticity in nanocomposites through patterned defects *Nat. Mater.* **14** 785–9
[14] Dickey M D 2017 Stretchable and soft electronics using liquid metals *Adv. Mater.* **29** 1606425
[15] Wang H, Lu W, Di J, Li D, Zhang X, Li M, Zhang Z, Zheng L and Li Q 2017 Ultra-lightweight and highly adaptive all-carbon elastic conductors with stable electrical resistance *Adv. Funct. Mater.* **27** 1606220
[16] Matsuhisa N, Inoue D, Zalar P, Jin H, Matsuba Y, Itoh A, Yokota T, Hashizume D and Someya T 2017 Printable elastic conductors by *in situ* formation of silver nanoparticles from silver flakes *Nat. Mater.* **16** 834
[17] Sekitani T, Noguchi Y, Hata K, Fukushima T, Aida T and Someya T 2008 A rubberlike stretchable active matrix using elastic conductors *Science* **321** 1468–72
[18] He S, Xu X M, Qiu X C, He Y and Zhou C H 2018 Conductivity of two-dimensional disordered nanowire networks: dependence on length-ratio of conducting paths to all nanowires *J. Appl. Phys.* **124** 054302
[19] Xia M G, Liang C P, Hu R X, Cheng Z F, Liu S R and Zhang S L 2018 Optimization of flexible substrate by gradient elastic modulus design for performance improvement of flexible electronic devices *Appl. Phys. Express* **11** 051601
[20] Choi S, Han S I, Kim D, Hyeon T and Kim D H 2019 High-performance stretchable conductive nanocomposites: materials, processes, and device applications *Chem. Soc. Rev.* **48** 1566–95
[21] Xu F and Zhu Y 2012 Highly conductive and stretchable silver nanowire conductors *Adv. Mater.* **24** 5117–22
[22] Kim D J, Shin H I, Ko E H, Kim K H, Kim T W and Kim H K 2016 Roll-to-roll slot-die coating of 400 mm wide, flexible, transparent Ag nanowire films for flexible touch screen panels *Sci. Rep.* **6** 34322
[23] Han K, Xie M L, Zhang L P, Yan L P, Wei J F, Ji G Q, Luo Q, Lin J, Hao Y Y and Ma C Q 2018 Fully solution processed semi-transparent perovskite solar cells with spray coated silver nanowires/ZnO composite top electrode *Solar Energy Mater. Solar Cells* **185** 399–405
[24] Jia L C, Yan D X, Liu X F, Ma R J, Wu H Y and Li Z M 2018 Highly efficient and reliable transparent electromagnetic interference shielding, film *ACS Appl. Mater. Interfaces* **10** 11941–9
[25] Kang L, Chen H, Yang Z J, Yuan Y B, Huang H, Yang B C, Gao Y L and Zhou C H 2018 Seesaw-like polarized transmission behavior of silver nanowire arrays aligned by off-center spin-coating *J. Appl. Phys.* **123** 205110
[26] Choi T Y, Hwang B U, Kim B Y, Trung T Q, Nam Y H, Kim D N, Eom K and Lee N E 2017 Stretchable, transparent, and stretch-unresponsive capacitive touch sensor array with selectively patterned silver nanowires/reduced graphene oxide electrodes *ACS Appl. Mater. Interfaces* **9** 18022–30
[27] Kim S R, Kim J H and Park J W 2017 Wearable and transparent capacitive strain sensor with high sensitivity based on patterned Ag nanowire networks *ACS Appl. Mater. Interfaces* **9** 26407–16
[28] Cui Z, Poblete F R and Zhu Y 2019 Tailoring the temperature coefficient of resistance of silver nanowire nanocomposites and their application as stretchable temperature sensors *ACS Appl. Mater. Interfaces* **11** 17836–42
[29] Yin F G, Lu H J, Pan H, Ji H J, Pei S, Liu H, Huang J Y, Gu J H, Li M Y and Wei J 2019 Highly sensitive and transparent strain sensors with an ordered array structure of AgNWs for wearable motion and health monitoring *Sci. Rep.* **9** 2403
[30] Xu X W, Liu Z F, He P and Yang J L 2019 Screen printed silver nanowire and graphene oxide hybrid transparent electrodes for long-term electrocardiography monitoring *J. Phys. D: Appl. Phys.* **52** 455401
[31] Peng Y Y, Du B Y, Xu X W, Yang J L, Lin J and Ma C Q 2019 Transparent triboelectric sensor arrays using gravure printed silver nanowire electrodes *Appl. Phys. Express* **12** 066503
[32] Gao M, Li L H and Song Y L 2017 Inkjet printing wearable electronic devices *J. Mater. Chem.* C **5** 2971–93
[33] Xie M *et al* 2018 Fully solution-processed semi-transparent perovskite solar cells with ink-jet printed silver nanowires top electrode *Solar RRL* **2** 1700184
[34] Li X, Lee G S, Park S H, Kong H, An T K and Kim S H 2018 Direct writing of silver nanowire electrodes via dragging mode electrohydrodynamic jet printing for organic thin film transistors *Org. Electron.* **62** 357–65
[35] Cui Z, Han Y W, Huang Q J, Dong J Y and Zhu Y 2018 Electrohydrodynamic printing of silver nanowires for flexible and stretchable electronics *Nanoscale* **10** 6806–11
[36] Yan P L, Brown E, Su Q, Li J, Wang J, Xu C X, Zhou C and Lin D 2017 3D printing hierarchical silver nanowire aerogel with highly compressive resilience and tensile elongation through tunable Poisson's ratio *Small* **13** 1701756
[37] Tu L, Yuan S J, Zhang H T, Wang P F, Cui X L, Wang J, Zhan Y Q and Zheng L R 2018 Aerosol jet printed silver nanowire transparent electrode for flexible electronic application *J. Appl. Phys.* **123** 174905
[38] Lu H, Lin J, Wu N, Nie S H, Luo Q, Ma C Q and Cui Z 2015 Inkjet printed silver nanowire network as top electrode for semi-transparent organic photovoltaic devices *Appl. Phys. Lett.* **106** 093302
[39] Peng Y Y, Xiao S G, Yang J L, Lin J, Yuan W, Gu W B, Wu X Z and Cui Z 2017 The elastic microstructures of inkjet printed polydimethylsiloxane as the patterned dielectric layer for pressure sensors *Appl. Phys. Lett.* **110** 261904